## PAPER

Check for updates

# Molecular building-blocks for anion–π interactions

Élise Antonetti, [iD] Yoann Cotelle, [iD] Alexandre Martinez [iD] and Paola Nava [iD] *

Theoretical calculations are performed to design a set of π molecules, significant for anion–π interactions. Quadrupole moments are reported at several levels of calculation. Trends from MP2 calculations are reproduced from DFT calculations, although actual values are different. Binding energies towards a chloride anion have been evaluated for the considered molecules and they roughly correlate with the quadrupole moment of the molecules, although other effects, such as structural flexibility, play a role. Imide moieties that decorate the π molecules provide privileged binding sites for anions; however, similar binding energies are obtained for the interaction between a chloride and benzenediimide, naphthalenediimide and perylenediimide, although quadrupole moments vary by a factor of two. The naphthalenediimide and the benzenetriimide emerge as valuable building blocks to construct extended molecular architectures with either $C_2$ or $C_3$ symmetry, for improved anion–π interactions and anion recognition.

## 1 Introduction

Anion–π interactions are non-covalent interactions that occur between negatively charged ions and electron-deficient π systems, showing a positive quadrupole moment. The first experimental evidence of their existence can be traced back to 2004,[1] although theoretical studies had already predicted their importance some years earlier.[2–4] Since then, anion–π interactions have attracted significant attention, as they have been shown to play a role in biological and chemical systems and in materials science.[5–13]

The nature of the anion–π interaction has been widely explored from theoretical and experimental points of view.[14–18] Early theoretical studies focus on the analysis of the interaction between anions and single-ring π systems, using various partition energy strategies, AIM (atoms in molecules) topological analysis, or electrostatic potential (ESP) maps.[10,16,19] Thus, substituted benzenes with electron-withdrawing groups,[3,4,20–22] as well as heterocycles or cyanuric acid derivatives,[2,14,23–25] have been identified as relevant molecular units. The anion–π interaction is predominantly due to electrostatic[22] and induction effects (anion-induced polarization of the π molecule)[20,24] and correlates with the quadrupole moment of the π molecule and its electrostatic potential.[26] The role of the substituents or heteroatoms in the π molecule has been highlighted by some authors: positive quadrupole moments and electrostatic potentials originate from the position of the nuclei, rather than from changes in the distribution of the

π-electron density itself.[25,27] Other aspects can be mentioned, such as the direct interaction between local C–X dipoles (X being a substituent or heteroatom),[27] or orbital relaxation and possible charge transfer, notably in the case of anion–carbonyl interactions.[28] The anion also has an influence on the nature of the interaction: computational energy decomposition analysis (EDA) together with UV-vis and X-ray crystallographic experiments suggest that stabilization in anion–π complexes with fluoro- or oxoanions is prevalently related to electrostatic terms, while orbital relaxation is important for halide anions.[29]

Experimental works have demonstrated interest in combining extended π systems with high quadrupole moments, based for instance on the naphthalenediimide unit, to achieve effective anion–π interactions.[5,8,10] Within supramolecular chemistry, anion–π interactions can be then exploited to propose artificial systems for the recognition and transport of anions of biological or environmental interest.[5,8–10] For instance, the chloride anion plays an important role in biological processes (ion homeostasis, cell volume regulation, transepithelial transport, and regulation of electrical excitability) and several receptors have been reported for this anion.[8,30,31] Anion–π interactions could also contribute to the stabilization of reaction intermediates or transition states, thus playing a role in catalytic transformation.[11–13] As such, a comparative study of extended π-acidic surfaces is appealing.

The purpose of this work is to computationally predict a scale of increasing anion–π interactions, focusing on the design of π systems. We systematically treat planar π molecules of increasing size, from single-rings to extended systems. Therefore, we explore a variety of molecular platforms that possess

*Aix Marseille Univ, CNRS, Centrale Med, iSm2, Marseille, France.*
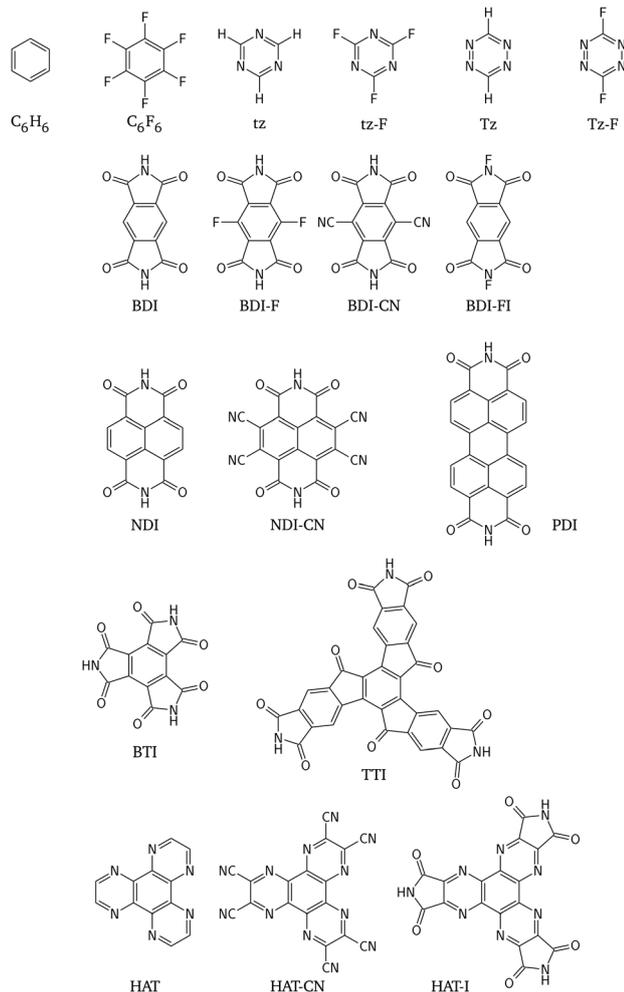*E-mail: paola.nava@univ-amu.fr*

This journal is © the Owner Societies 2025

*Phys. Chem. Chem. Phys.*, 2025, **27**, 17997–18004 | 17997

Fig. 1 Molecules treated in this work, and labels.

symmetry $C_2$ or $C_3$, which are potential candidates for the conception of elaborated molecular architectures. Our systematic approach is desirable and meaningful because it allows for direct comparison between the properties of the considered systems, all treated on the same footing. Starting from single-ring molecules (top of Fig. 1), extended π systems were constructed, which have been proven to be significant for anion–π interactions.[5,11] From the benzene ring, the benzenediimide molecule (BDI) is built formally by adding two cyclic imides. The BDI platform has been modified by introducing fluorine or cyano groups on the central ring or by modifying the imide moiety. The π system is further extended to obtain NDI- and PDI-based molecules (NDI = naphthalenediimide, PDI = perylenediimide). The benzenetriimide (BTI) is constructed by adding three cyclic imides to the central benzene, while the truxenonetriimide (TTI) contains three more extended π arms.[32] Finally, we considered systems derived from 1,4,5,8,9,12-hexaazatriphenylene (HAT).[33,34] For all of these molecules, quadrupole moments and polarizability values are provided, computed at several theoretical levels. We have then studied the interaction of these π molecules with a prototypical anion, the chloride.

The binding energies and preferred binding sites are analyzed in light of the properties of isolated π molecules, by exploiting the electrostatic surface potential maps and computed charges.

## 2 Computational details

Density functional theory (DFT) and MP2 calculations were carried out using the TURBOMOLE program package.[35] The structures were optimized at each computational level in the gas phase.

MP2 calculations employ the aug-cc-pVTZ basis set and the corresponding auxiliary basis sets for the resolution of identity (RI) approximation.[36,37] Diffuse functions were omitted on hydrogen atoms (cc-pVTZ for H) for the TTI case,[38] to avoid convergence issues. In the case of small, single-ring molecules, CCSD(T) calculations were also performed to check polarizability values. For this purpose, the MOLPRO program package was used[39] and polarizabilities were computed numerically (see the SI for details on the basis set and polarizabilities).

For DFT calculations, the def2-TZVP basis set was employed throughout, together with the corresponding auxiliary basis sets for the RI technique.[40,41] Several functionals were tested for calculations of the quadrupole moments and polarizabilities of the molecules shown in Fig. 1: PBE0,[42–46] B3LYP,[42,43,47–50] CAM-B3LYP,[51] M06, M062X,[52] WB97XD[53] and SCLH22T.[54] For PBE0, B3LYP and CAM-B3LYP, the D3 empirical dispersion corrections were added.[55] Frequency calculations were performed on the PBE0-D3 structures to verify the nature of the stationary points, which are proved to be minima on their potential energy surface at this level of computation. In all cases, we report the $Q_{zz}$ component of the quadrupole tensor, obtained by maintaining the π system in the $xy$ plane.

Calculations of the interaction between the π systems and the chloride anion were performed at the levels of MP2, PBE0-D3 and SCLH22T only. Frequency calculations were performed on the PBE0-D3 adduct structures. The interaction is discussed in terms of binding energies $\Delta E$, defined as follows:

$$\Delta E = E_{\pi\text{–Cl}^-} - E_\pi - E_{\text{Cl}^-} \qquad (1)$$

where $E_{\pi\text{–Cl}^-}$, $E_\pi$, and $E_{\text{Cl}^-}$ refer to the total electronic energies of the adduct, the isolated π system and the isolated chloride, respectively. The reported values $\Delta E$ are corrected for the basis set superposition error (BSSE) using the counterpoise method. Uncorrected results are available in the SI.

## 3 Results and discussion

### 3.1 Quadrupole moments and polarizabilities

Table 1 collects results from computed MP2 $Q_{zz}$ values for all treated systems, as well as polarizabilities at the MP2 and CCSD(T) levels for single-ring molecules. Concerning quadrupole moments, our MP2 values are comparable to those reported in previous works at a similar level of computation: they are within 0.5 DÅ with respect to the MP2 values reported by Doerksen et al.,[56] employing a basis set optimized for

17998 | Phys. Chem. Chem. Phys., 2025, 27, 17997–18004

This journal is © the Owner Societies 2025

**Table 1** Computed $Q_{zz}$ (DÅ) values at the MP2/aug-cc-pVTZ level (unrelaxed values in parenthesis). Polarizabilities (a.u.) are reported at the MP2 and CCSD(T) levels. Selected values from previous contributions are reported, as well as experimental data, if available. Labels as in Fig. 1

| | $Q_{zz}$ (DÅ) | | $\alpha_{\parallel}$ (a.u.) | | |
|---|---|---|---|---|---|
| System | MP2 | Lit.[a] | MP2 | CCSD(T) | Lit.[a] |
| $C_6H_6$[b] | −7.97 (−8.71) | −7.99[56] | 45.0 | 44.5 | 47.5[23] |
| tz[b] | 0.84 (0.40) | 0.90[14,56] | 33.9 | 33.6 | 30.3[14] |
| Tz | 3.31 (2.60) | 3.32[56] | 32.2 | 32.3 | 58.7[23] |
| $C_6F_6$[b] | 8.04 (9.26) | | 42.5 | 42.2 | |
| tz-F | 8.07 (8.64) | 8.23[14] | 33.5 | 33.3 | 30.3[14] |
| Tz-F | 8.28 (8.31) | | 32.2 | 32.3 | |
| BDI | 11.25 (14.23) | | | | |
| BDI-F | 14.73 (18.10) | | | | |
| BDI-FI | 23.19 (27.52) | | | | |
| BDI-CN | 24.39 (27.60) | | | | |
| NDI | 13.68 (16.67) | 14.7[57] | | | |
| NDI-CN | 53.17 (57.72) | 55.5[58] | | | |
| PDI | 21.00 (27.29) | | | | |
| BTI | 17.24 (21.52) | 14.5[59] | | | |
| TTI[c] | 36.25 (46.66) | | | | |
| HAT | −8.79 (−10.72) | −8.53[16] | | | 54.0[16] |
| HAT-I | 27.04 (34.95) | | | | |
| HAT-CN | 75.12 (80.10) | | | | |

[a] Computational levels: ref. 56: MP2/[5s3p2d/3s2p]//MP2/6-31G(d); ref. 14: MP2/6-31G* for $Q_{zz}$ and MP2/6-31++G** for $\alpha_{\parallel}$; ref. 57 and 58: MP2/6-311G**//PBE0/6-311++G**; ref. 23: MP2/6-311+G**. [b] Exp. $Q_{zz}$ for $C_6H_6$: −8.69 ± 0.5, gas phase;[60] −8.48 ± 0.36, in CCl₄.[61] For tz: −0.83 ± 0.93 in $C_6H_{12}$;[62] −1.05 ± 0.17 from X-ray.[63] For $C_6F_6$: 9.5 ± 0.5, gas phase.[60] [c] cc-pVTZ basis for H atoms.

polarizabilities; they are within 2 DÅ with respect to the values from experiments. The largest discrepancy is for the BTI system,[59] but we believe that the reported value was not computed at the MP2 level. DFT results are reported in Fig. 2 and Table 2. The computed unsigned values are systematically lower than those obtained at the MP2 level. However, and satisfactorily, the DFT methods reproduce the MP2 trends, as visualized by the regression line in Fig. 2 for PBE0-D3 ($R^2 = 0.9996$). Similar behaviors are observed for the other functionals, as detailed in Table 2: $R^2$ values are always larger than 0.997.
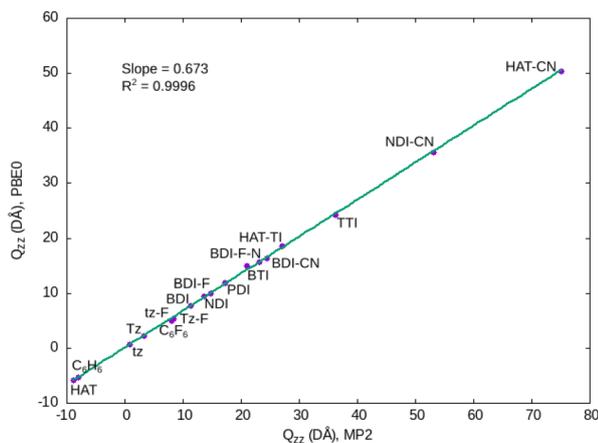


**Fig. 2** Correlation curve between quadrupole moments $Q_{zz}$ (DÅ) computed at the MP2 and PBE0-D3 levels. Labels for molecules as in Fig. 1.

Expanding the benzene ring to BDI, thus adding cyclic imides, has a large effect on $Q_{zz}$, which increases from −7.97 (benzene) to 11.25 DÅ (BDI, MP2 values). Substitutions on the BDI have also an impact: the quadrupole moment increases by 3.5 DÅ by replacing the hydrogen by fluorine atoms on the central 6-membered ring. Interestingly, the $Q_{zz}$ values become more than twice larger, either by introducing cyano groups on the central ring, or by modifying N–H to N–F in the imide moiety. The extension of the aromatic core from BDI to NDI increases the $Q_{zz}$ value only slightly. The increase is more pronounced for PDI, with a value of $Q_{zz}$ close to that of BDI-CN. Again, and as expected,[5,11] the effect of the cyano substitution is evident when comparing NDI and NDI-CN. The computed quadrupole moment of the NDI-CN (MP2: 53.17 DÅ) is comparable to the previously reported value for a similar structure (55.5 DÅ computed for an N-substituted tetraciano-NDI).[58]

A value of $Q_{zz}$ of 17.24 DÅ (MP2 value) is associated with the BTI molecule, which contains three cyclic imide moieties, and thus is higher than the value obtained for BDI. The value of $Q_{zz}$ increases considerably to 36.25 DÅ for the TTI molecule. The HAT system has a negative $Q_{zz}$. By decorating it with three cyclic imide moieties or cyano groups, positive $Q_{zz}$ values are obtained.

Concerning polarizabilities,[14,16,23] MP2 values for small systems are the same as those obtained at the CCSD(T) level (within 0.5 a.u.), Table 1. The values obtained from DFT (PBE0-D3), Table 2, are underestimated, but trends are respected. Previously, it has been argued that the s-tetrazine has a significant larger polarizability than benzene (58.7 a.u. and 47.5 a.u., respectively at the MP2 level).[23] However, from high accurate CCSD(T) calculations we conclude that benzene has the largest polarizability (44.5 a.u.) among the six single-ring molecules studied and that the s-tetrazine has a similar polarizability to s-triazine (32.3 a.u. and 33.6, respectively), thus lower than that of benzene, Table 1. Fluorine substitution has no impact on polarizabilities; however, Tables 1 and 2, while introducing cyano groups increases them slightly. The effect is much larger when imide groups are introduced (DFT values, Table 2), as can be seen by comparing benzene (38.60 a.u.) to BDI (63.75 a.u.), BDI to BTI (76.19 a.u.), or HAT (79.93 a.u.) to HAT-I (118.23 a.u.). Finally, extending the π system from BDI to HAT and then to NDI, PDI and TTI has the greatest effect on polarizability, which then rises up to 172.4 a.u. (PBE0-D3) for TTI, Table 2.

### 3.2 Interaction with an anion

To go a step further, the structures of the adducts between the considered π molecules and the chloride were optimized to evaluate the binding energies and correlate them with the calculated quadrupole moments of the π molecules. Moreover, although the computed positive values $Q_{zz}$ suggest favorable interactions with anions, they do not provide information about the preferred binding sites. For small molecules, from benzene to difluoro-s-tetrazine, the chloride has been forced to be on the $Oz$ axis, to avoid other interactions, i.e. hydrogen

**Table 2** $Q_{zz}$ (DÅ) values obtained at several DFT levels of calculation, def2-TZVP basis set. Intercept, slope and $R^2$ from the linear regression with relaxed-MP2 values for $Q_{zz}$ are indicated, as for PBE0-D3 in Fig. 2. Polarizabilities (a.u.) are reported at the PBE0-D3 level. Labels are as given in Fig. 1

| System | $Q_{zz}$ (DÅ) | | | | | | | $\alpha_{\parallel}$ (a.u.) |
| | PBE0-D3 | M06 | M062X | WB97XD | CAM-B3LYP-D3 | B3LYP | SCLH22T | PBE0-D3 |
|---|---|---|---|---|---|---|---|---|
| $C_6H_6$ | −5.43 | −4.94 | −5.48 | −5.41 | −5.26 | −5.26 | −5.27 | 38.60 |
| tz | 0.58 | 0.87 | 0.48 | 0.61 | 0.72 | 0.74 | 0.70 | 29.71 |
| Tz | 2.14 | 2.34 | 2.04 | 2.17 | 2.28 | 2.29 | 2.27 | 28.49 |
| $C_6F_6$ | 4.92 | 5.29 | 5.31 | 5.17 | 5.69 | 5.55 | 5.72 | 38.17 |
| tz-F | 5.18 | 5.30 | 5.38 | 5.27 | 5.58 | 5.52 | 5.64 | 29.36 |
| Tz-F | 5.35 | 5.45 | 5.44 | 5.43 | 5.69 | 5.61 | 5.72 | 28.53 |
| BDI | 7.65 | 8.20 | 7.64 | 7.88 | 8.54 | 8.49 | 8.38 | 63.75 |
| BDI-F | 9.95 | 10.54 | 10.00 | 10.23 | 10.96 | 10.84 | 10.76 | 63.78 |
| BDI-FI | 15.64 | 16.47 | 16.02 | 16.10 | 16.96 | 16.73 | 16.87 | 64.02 |
| BDI-CN | 16.39 | 17.04 | 16.29 | 16.80 | 17.63 | 17.36 | 17.36 | 75.60 |
| NDI | 9.37 | 10.28 | 9.23 | 9.57 | 10.42 | 10.55 | 10.18 | 81.48 |
| NDI-CN | 35.65 | 36.75 | 35.62 | 36.50 | 37.74 | 37.20 | 37.35 | 105.25 |
| PDI | 14.95 | 16.45 | 14.39 | 14.97 | 16.53 | 17.15 | 16.24 | 125.48 |
| BTI | 11.80 | 12.46 | 11.76 | 12.16 | 13.04 | 12.85 | 12.78 | 76.19 |
| TTI | 24.16 | 25.92 | 24.30 | 25.04 | 27.47 | 27.22 | 26.45 | 172.43 |
| HAT | −5.84 | −4.55 | −6.38 | −5.86 | −5.40 | −5.08 | −5.84 | 79.93 |
| HAT-I | 18.50 | 19.69 | 18.57 | 18.97 | 20.54 | 20.25 | 19.97 | 118.23 |
| HAT-CN | 50.43 | 51.55 | 50.34 | 51.53 | 52.74 | 51.82 | 52.36 | 116.56 |
| Intercept | 0.010 | 0.562 | −0.038 | 0.058 | 0.524 | 0.625 | 0.407 | |
| Slope | 0.673 | 0.684 | 0.674 | 0.688 | 0.707 | 0.695 | 0.700 | |
| $R^2$ | 0.9996 | 0.9981 | 0.9998 | 0.9997 | 0.9981 | 0.9971 | 0.9990 | |

**Table 3** MP2, PBE0-D3 and SCLH22T binding energies of the chloride, $\Delta E$ (kJ mol$^{-1}$), as defined in eqn (1). D3 empirical dispersion parameters were employed for PBE0 calculations. The binding sites are denoted as $s_A$ (imide site), $s_B$ (TTI case) and $s_C$ (central ring), Fig. 3

| Complex | Site | MP2 | PBE0-D3 | SCLH22T |
|---|---|---|---|---|
| $C_6H_6$ | $s_C{}^a$ | 1.6 | 8.4 | 8.4 |
| tz | $s_C{}^a$ | −32.5 | −27.7 | −26.5 |
| Tz | $s_C{}^a$ | −45.3 | −40.4 | −39.0 |
| $C_6F_6$ | $s_C$ | −62.0 | −55.3 | −57.4 |
| tz-F | $s_C$ | −72.2 | −67.9 | −68.9 |
| Tz-F | $s_C{}^a$ | −75.4 | −69.0 | −70.3 |
| BDI | $s_A$ | −86.3 | −91.1 | −85.3 |
| BDI-F | $s_A$ | −102.2 | −108.9 | −104.1 |
| BDI-FI | $s_A$ | −118.9 | −123.0 | −118.4 |
| BDI-CN | $s_A$ | −136.8 | −147.3 | −140.6 |
| NDI | $s_A$ | −91.6 | −94.3 | −87.7 |
| NDI-CN | $s_A$ | −185.3 | −200.4 | −191.9 |
| PDI | $s_C$ | −90.7 | −91.1 | −81.7 |
| PDI | $s_A$ | −85.5 | −91.3 | −82.1 |
| BTI | $s_A$ | −112.6 | −119.2 | −111.9 |
| TTI | $s_B$ | −150.5 | −151.3 | −144.0 |
| TTI | $s_A$ | −97.2 | −113.9 | −105.2 |
| TTI$^a$ | $s_C{}^a$ | −122.0 | −111.1 | −104.3 |
| HAT | $s_C$ | −65.1 | −58.1 | −49.4 |
| HAT-I | $s_A$ | −152.2 | −153.0 | −144.0 |
| HAT-I | $s_C$ | −135.7 | −143.0 | −133.5 |
| HAT-CN | $s_C$ | −216.0 | −222.5 | −215.4 |

$^a$ Imaginary frequencies due to imposed constraints.



**Fig. 3** Top view of the chloride binding sites. Green circles indicate positions close to the imide ($s_A$), orange circles are on the most central rings ($s_C$), and the blue circle indicates a site close to the cyclopentenone moiety ($s_B$).

Imide sites $s_A$
(BDI-, NDI-based systems, BTI)

PDI: $s_A$; $s_C$

TTI: $s_A$, $s_B$, $s_C$

HAT-based: $s_A$; $s_C$

bonding. In some cases, due to the applied constraints, imaginary frequencies appear, Table 3.

For π systems containing fused rings, several structures were fully optimized to identify anion binding sites, Fig. 3 and Table 3. The chloride was approached along the $z$ axis, *e.g.* from above the π system, to avoid structures in which the anion interacts with a hydrogen atom in the molecular plane. In most cases, the preferred (and sometimes unique) binding site is on
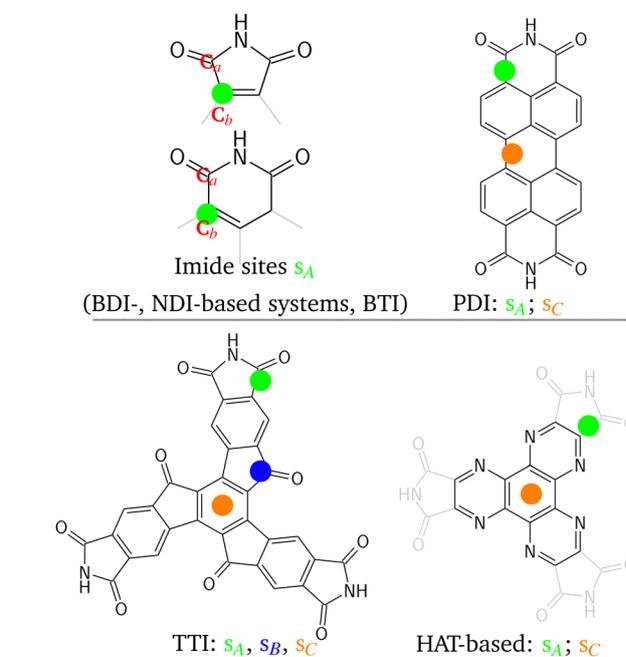
top of the imide unit, usually displaced to the $C_a$–$C_b$ bond, where $C_a$ is the carbon atom of the carbonyl moiety (green sites, $s_A$, Fig. 3): BDI-based systems, NDI-based systems, BTI and HAT-I. In the case of the PDI platform, we identify two sites that lead to very close $\Delta E$: in addition to the site close to the imide ($s_A$ in green, $\Delta E = -85.5$ kJ mol$^{-1}$), a second binding site leads to an adduct with a $\Delta E = -90.7$ kJ mol$^{-1}$ ($s_C$ in orange, MP2 values). For the TTI molecule we investigated three

**18000** | *Phys. Chem. Chem. Phys.*, 2025, **27**, 17997–18004

This journal is © the Owner Societies 2025

possibilities: the site close to the imide ($s_A$ in green, MP2 $\Delta E$ = −97.2 kJ mol$^{-1}$); the site close to the cyclopentenone moiety ($s_B$ in blue, MP2 $\Delta E$ = −150.5 kJ mol$^{-1}$); finally, the approach on the $C_3$ axis was also calculated ($s_C$ in orange, MP2 $\Delta E$ = −122.0 kJ mol$^{-1}$). In the case of the HAT-based derivatives, a site on the central ring was obtained, and, in the case of the HAT-I platform, the imide position was retrieved as well.

Interestingly, the binding sites are consistent with the results from both NBO and Hirshfeld charges, and the ESP maps, evaluated for isolated π molecules, and shown for the BDI, TTI and HAT cases in Fig. 4. Accordingly, the carbon atoms with the highest computed charges are those close to the imide moieties for BDI. For the TTI system, two sites emerge, *e.g.* close either to the imide or to the carbonyl of the cyclopentenone. The full data for all treated molecules are available in the SI.

Concerning methods, the MP2 trends on $\Delta E$ are reproduced by the DFT approaches, as shown by the regression lines in the SI ($R^2$ = 0.987 for both PBE0-D3 and SCLH22T). We notice that the PBE0-D3 values for the $s_C$ sites are often slightly larger, while the PBE0-D3 methods usually overstabilize the complexes at the imide sites $s_A$ with respect to MP2. Consequently, the PBE0-D3 calculated distances for Cl–C$_a$ and Cl–C$_b$ are significantly shorter

**Table 4** MP2 and PBE0-D3 computed distances (pm) between the chloride and the carbon atoms close to the imide binding sites, Fig. 3

| System | MP2 | | PBE0-D3 | |
|---|---|---|---|---|
| | Cl–C$_a$ | Cl–C$_b$ | Cl–C$_a$ | Cl–C$_b$ |
| BDI | 294.06 | 292.11 | 278.10 | 278.13 |
| BDI-F | 287.16 | 278.19 | 279.02 | 269.73 |
| BDI-FI | 275.07 | 278.35 | 270.77 | 268.61 |
| BDI-CN | 279.95 | 258.03 | 276.80 | 253.64 |
| NDI | 313.82 | 309.43 | 283.37 | 280.61 |
| NDI-CN | 279.19 | 245.61 | 275.42 | 239.25 |
| PDI | 304.91 | 297.54 | 285.09 | 276.75 |
| BTI | 289.89 | 269.44 | 282.36 | 262.84 |
| TTI | 286.36 | 274.81 | 279.22 | 259.28 |
| HAT-I | 282.04 | 244.45 | 278.36 | 242.40 |

than in MP2, Table 4. In apparent contrast with our results, previous reports show that DFT provides longer distances and lower stabilization energies (in absolute value) than MP2. This difference is due to the fact that we included dispersion corrections in our DFT calculations, which contribute to the stabilization of the anion–π complexes.[3,10]

The plot in Fig. 5 collects the MP2 computed values $\Delta E$ for the most stable adducts as a function of the $Q_{zz}$ of the corresponding π systems. The interaction between the anion and the π molecule roughly follows the quadrupole moment, as the values of $\Delta E$ decrease with increasing $Q_{zz}$. However, the regression line with an $R^2$ = 0.877, lower than 0.95, suggests that the quadrupole moment is not the only factor that affects the binding energies and prompted us to further analyze the computed data.

First of all, the HAT molecule has a remarkably low $\Delta E$, despite its negative $Q_{zz}$. This can be understood by inspecting the ESP map, Fig. 4, which reveals that the electrostatic potential is positive on the carbon atoms of the central ring and associated charges are also positive.

Let us now focus on the systems where the anion approaches from the top of the imide sites ($s_A$, green cases in Fig. 5). From
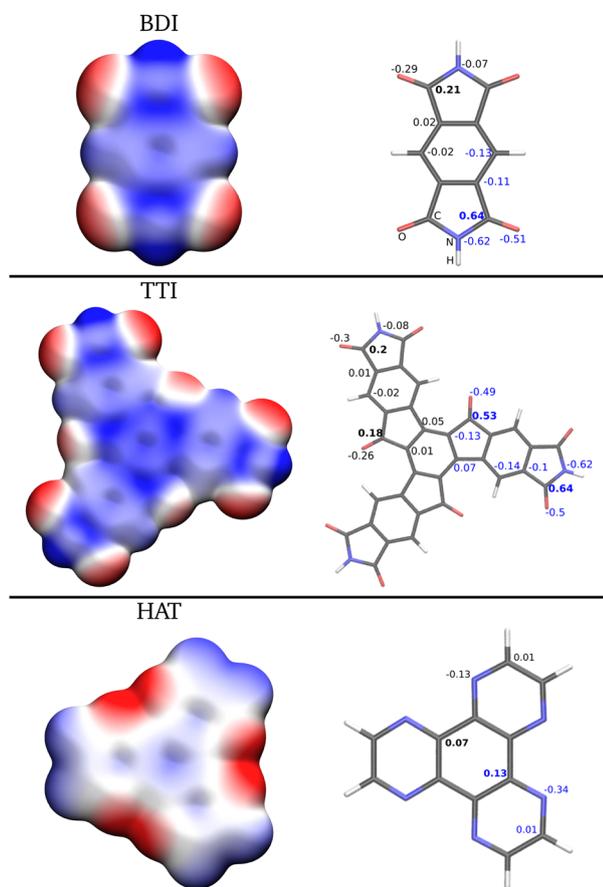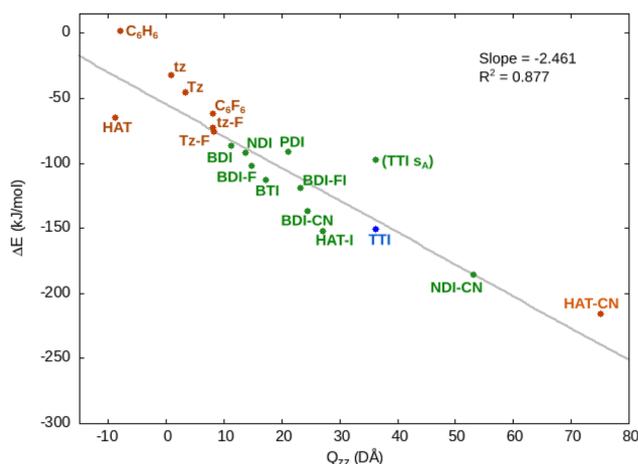


**Fig. 4** Electrostatic potential maps for selected π systems, mapped on the electron density iso-surface of 0.001 a.u. The red color corresponds to a negative region of the electrostatic potential (−0.04 a.u.), whereas the blue color corresponds to the region where the potential is positive (+0.04 a.u.). Charges (NBO in blue and Hirshfeld in black) are indicated for heteroatoms.



**Fig. 5** Smallest MP2 computed $\Delta E$ values (among the tested adduct structures) as a function of the $Q_{zz}$ of each π system. Orange, green and blue dots refer to $s_C$, $s_A$ and $s_B$ binding sites, as in Fig. 3. The value for the TTI $s_A$ case is also reported (but not used for the regression).

This journal is © the Owner Societies 2025

*Phys. Chem. Chem. Phys.*, 2025, **27**, 17997–18004 | **18001**

the point of view of the structures, the MP2 distances between the chloride anion and carbon atoms $C_a$ and $C_b$ vary between 244 and 314 pm and are sensitive to substitutions, Table 4. The $Cl–C_b$ distances are usually shorter than the corresponding $Cl–C_a$ distances, indicating that the anion position is slightly displaced toward the $C_b$ atom. In this way, repulsive interactions between the anion and the nitrogen or oxygen atoms of the imide moiety are minimized. The $Cl–C_a$ distance becomes shorter when NDI and NDI-CN are compared, or within the BDI, BDI-F and BDI-CN series. Substitution with the electron-withdrawing group (–CN or –F) is performed in the β position: it affects the strength of the interaction, but the electron-withdrawing group is sufficiently far from $C_a$, and repulsion with the incoming anion is therefore avoided. Thus, when comparing NDI and NDI-CN, $Q_{zz}$ increases and $\Delta E$ decreases. Again, within the series BDI, BDI-F and BDI-CN (substitutions with electron-withdrawing groups), the $Q_{zz}$ values increase and the $\Delta E$ values decrease. Similarly, $\Delta E$ decreases from BDI to BTI (from two to three imide moieties). However, and interestingly, the binding energies are close for BDI, NDI, and PDI, although the PDI molecule has a significantly larger quadrupole moment. In addition, there is no improvement for the TTI ($s_A$ site) compared to the BTI.

The TTI system is instructive: the preferred binding site is close to the ketone in the cyclopentenone (blue site in Fig. 3, $s_B$), although the calculated charge is slightly higher for the carbon atom in the imide moiety, Fig. 4. Inspection of the PBE0-D3 adduct geometries, Fig. 6, reveals that the $Cl–C_a$ distance in $s_A$ (279 pm) is significantly longer than $Cl–C_2$ in $s_B$ (252 pm) and that there is more structural flexibility close to the binding site in $s_B$ than in $s_A$. Approaching the anion causes a distortion in the planarity of the π molecule, which is more significant for the $s_B$ adduct. It could be argued that the binding energy results from the modification of the π system, meaning that it would essentially be due to the negative charge interacting with the induced dipole moment of the modified π system. Yet, the dipole moments of the neutral π molecules in the geometry of the chloride adducts, Table 5 for TTI and BDI, are quite small, although the values for TTI site $s_B$ are, as expected, slightly higher (dipole moment values for all π systems are available in the SI). We then evaluated the binding energies for adducts, where we constrained the planarity of the binding site.
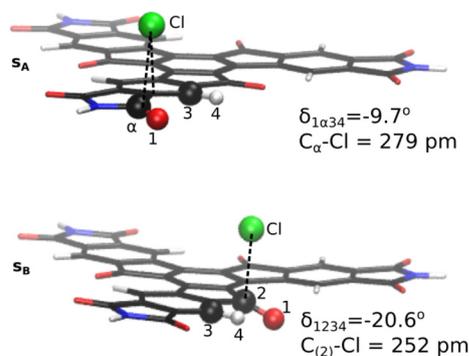
**Table 5** Dipole moments (D) of the neutral π molecules in the geometry of the unconstrained adducts (left) and the adducts with constrained planarity (right). PBE0-D3 binding energies are also reported (kJ mol⁻¹)

| System | Unconstrained adduct | | Adduct with constrained planarity | |
|---|---|---|---|---|
| | $\Delta E$ | Dipole | $\Delta E$ | Dipole |
| BDI | −91.1 | 0.54 | −84.4 | 0.07 |
| TTI $s_A$ | −113.9 | 0.46 | −107.1 | 0.10 |
| TTI $s_B$ | −151.3 | 0.67 | −140.6 | 0.19 |

In all cases, the so-obtained binding energies are only up to 11 kJ mol⁻¹ higher than in the optimized structures, and the global gain in energy from the anion–dipole interaction that compensates for the deformation of the π structure is rather small. Finally, energy decomposition analysis (EDA) was used to compare the $s_B$ and $s_A$ adducts, Fig. 7. This analysis was also performed on a structure where the $Cl–C_a$ distance is shortened up to 252 pm ($s_A(252)$ structure in Fig. 7), which is the $Cl–C_2$ distance in $s_B$ (results of further constrained structures are collected in the SI). In this approach, the interaction energy $\Delta E$ is decomposed into several contributions: $\Delta E = E_{\text{exc-rep}} + E_{\text{elec}} + E_{\text{or}} + E_{\text{corr}} + E_{\text{disp}}$. Stabilizing contributions from correlation ($E_{\text{corr}}$) and dispersion ($E_{\text{disp}}$) terms are similar in all cases. The favorable binding energies $\Delta E$ originate primarily from the compensation between positive repulsive contributions ($E_{\text{exc-rep}}$) on the one side and negative electrostatic ($E_{\text{elec}}$) and orbital relaxation ($E_{\text{or}}$) contributions on the other side. By approaching the chlorine anion towards the $C_a$ atom, we recover the same electrostatic and orbital relaxation terms as in the $s_B$ adduct, but the repulsion contribution has clearly increased. This suggests that the approach of the anion at the $s_A$ site is somewhat limited by the structural rigidity of the imide moiety and the repulsive interactions that arise. Thus, the more favorable $\Delta E$ calculated for the site $s_B$ than $s_A$ results from structural flexibility and from the fact that repulsive interactions in $s_A$ prevent the anion from getting close to the $C_a$ atom.



**Fig. 6** PBE0-D3 optimized structures of the adduct between the chloride and the TTI molecule, sites $s_A$ and $s_B$.
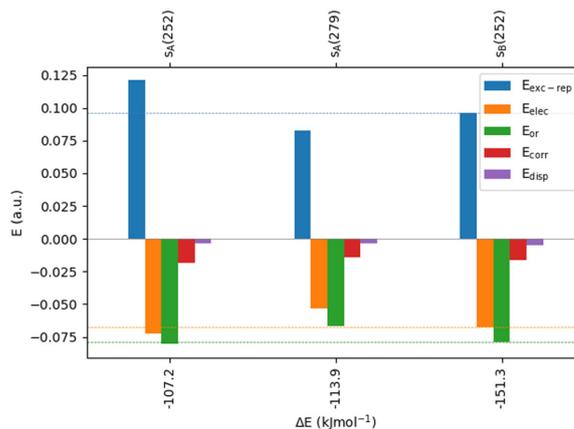


**Fig. 7** Energy decomposition analysis performed on the PBE0-D3 optimized structures of the adduct between a chloride and the TTI molecule, sites $s_A$ and $s_B$, denoted $s_A(279)$ and $s_B(252)$. In the $s_A(252)$ structure the $Cl–C_a$ distance is 252 pm. The terms of the decomposition are given in the main text.

**18002** | *Phys. Chem. Chem. Phys.*, 2025, **27**, 17997–18004

This journal is © the Owner Societies 2025

# 4 Conclusions

In the present study, we report a comprehensive and systematic study of π molecules significant for anion–π interactions.

First, we report a corrected value for the polarizability of the *s*-tetrazine ($\alpha_\parallel$ = 32.3 a.u., CCSD(T) level). Concerning quadrupole moments, we show that DFT calculations with a set of def2-TZVP bases provide correct trends compared to MP2-computed reference results, although absolute values may differ significantly. Thus, care should be taken when comparing computed quadrupole moments from different sources if the methods used are not the same or if the computational levels are unclear. Moreover, we establish a linear relationship between MP2 and DFT results. This suggests that, by providing the coefficients of the regression line, quadrupole moments of MP2 quality can be extrapolated from a simple DFT run, thus avoiding the actual MP2 calculation, the convergence of which is tedious for extended systems together with diffuse basis functions.

The interaction between a chloride anion and π molecules has been investigated by evaluating the binding energies. Computed charges and ESP maps are convenient tools for predicting possible binding sites of an anion on a neutral molecular structure, and they could be particularly useful when dealing with extended, non-planar molecules. As expected, the binding energies decrease roughly with the quadrupole moments of the π molecules. However, equilibrium geometries and binding energies result from a compromise between several factors, including local structural rigidity. Interestingly, imide moieties provide privileged binding sites for anions, but BDI, NDI, and PDI, or BTI and TTI display similar binding energies (on the imide binding site), although the quadrupole moments are different. The binding energy clearly decreases by performing a β-substitution on the imide carbon atom, such as for BDI-CN in comparison to BDI. Alternatively, the decrease in binding energy is evident when BDI is compared to BTI, thus introducing another imide moiety on the π platform.

In the case of the TTI molecule, three binding sites have been evaluated. The most favorable site, $s_B$, is close to the carbonyl moiety near the central ring. It offers more structural flexibility and less repulsive interactions than the $s_A$ site. These aspects – structural flexibility and repulsive interactions between the incoming anion and heteroatoms – also emerge as factors that affect the anion–π interaction strength.

Finally, the π platforms that are presented in this study are suitable to promote anion–π interactions. Among them, NDI emerges as a privileged choice to conceive extended molecular architectures with $C_2$ symmetry, for improved anion–π interactions and anion recognition. Similarly, BTI turns out to be the best candidate as a $C_3$-symmetry building block. In fact, it has recently been used to synthesize molecular cages that combine such a platform with an electron-rich cyclotriveratrylene (CTV).[64,65] The TTI molecule remains an attractive alternative that offers a more extended structural core than BTI.

# Conflicts of interest

There are no conflicts to declare.

# Data availability

Details of MP2 and CCSD(T) calculations, computed binding energies, details of structural parameters, EDA on TTI structures, all ESP maps and charges, coordinates. See DOI: **https://doi.org/10.1039/d5cp01879j**

The data supporting this article have been included as part of the SI.

# Acknowledgements

# Notes and references

1 P. de Hoog, P. Gamez, I. Mutikainen, U. Turpeinen and J. Reedijk, *Angew. Chem.*, 2004, **116**, 5939–5941.

2 M. Mascal, A. Armstrong and M. D. Bartberger, *J. Am. Chem. Soc.*, 2002, **124**, 6274–6276.

3 I. Alkorta, I. Rozas and J. Elguero, *J. Am. Chem. Soc.*, 2002, **124**, 8593–8598.

4 D. Quiñonero, C. Garau, C. Rotger, A. Frontera, P. Ballester, A. Costa and P. M. Deyà, *Angew. Chem., Int. Ed.*, 2002, **41**, 3389–3392.

5 R. E. Dawson, A. Hennig, D. P. Weimann, D. Emery, V. Ravikumar, J. Montenegro, T. Takeuchi, S. Gabutti, M. Mayor, J. Mareda, C. A. Schalley and S. Matile, *Nat. Chem.*, 2010, **2**, 533–538.

6 X. Lucas, A. Bauzá, A. Frontera and D. Quiñonero, *Chem. Sci.*, 2016, **7**, 1038–1050.

7 Z. Huang, Y. Bai, X. Huang, J. Li, Y. Wu, Y. Chen, K. Li, X. Niu, N. Li, G. Liu, Y. Zhang, H. Zai, Q. Chen, T. Lei, L. Wang and H. Zhou, *Nature*, 2023, **623**, 531–537.

8 V. Gorteau, G. Bollot, J. Mareda, A. Perez-Velasco and S. Matile, *J. Am. Chem. Soc.*, 2006, **128**, 14788–14789.

9 Z. Xu, N. J. Singh, S. K. Kim, D. R. Spring, K. S. Kim and J. Yoon, *Chem. – Eur. J.*, 2011, **17**, 1163–1170.

10 I. A. Rather, S. A. Wagay and R. Ali, *Coord. Chem. Rev.*, 2020, **415**, 213327.

11 C. Wang, F. N. Miros, J. Mareda, N. Sakai and S. Matile, *Angew. Chem., Int. Ed.*, 2016, **55**, 14422–14426.

12 A.-B. Bornhof, A. Bauzá, A. Aster, M. Pupier, A. Frontera, E. Vauthey, N. Sakai and S. Matile, *J. Am. Chem. Soc.*, 2018, **140**, 4884–4892.

13 Y. Zhao, Y. Domoto, E. Orentas, C. Beuchat, D. Emery, J. Mareda, N. Sakai and S. Matile, *Angew. Chem., Int. Ed.*, 2013, **52**, 9940–9943.

14 C. Garau, A. Frontera, D. Quiñonero, P. Ballester, A. Costa and P. M. Deyà, *ChemPhysChem*, 2003, **4**, 1344–1348.

15 D. Y. Kim, N. J. Singh, J. W. Lee and K. S. Kim, *J. Chem. Theory Comput.*, 2008, **4**, 1162–1169.

16 B. L. Schottel, H. T. Chifotides and K. R. Dunbar, *Chem. Soc. Rev.*, 2007, **37**, 68–83.

This journal is © the Owner Societies 2025

*Phys. Chem. Chem. Phys.*, 2025, **27**, 17997–18004 | **18003**

17 A. Frontera, P. Gamez, M. Mascal, T. J. Mooibroek and J. Reedijk, *Angew. Chem., Int. Ed.*, 2011, **50**, 9564–9583.

18 S. V. Rosokha, *ChemPlusChem*, 2023, **88**, e202300350.

19 O. Zayene, R. Plais, L. Rolhion, F. Bourdreux, G. Pieters, A. Gaucher, G. Clavier, A. Cœuret, J.-Y. Salpin and D. Prim, *ChemistrySelect*, 2024, **9**, e202302763.

20 D. Kim, P. Tarakeshwar and K. S. Kim, *J. Phys. Chem. A*, 2004, **108**, 1250–1258.

21 D. Y. Kim, N. J. Singh and K. S. Kim, *J. Chem. Theory Comput.*, 2008, **4**, 1401–1407.

22 J. Thirman and M. Head-Gordon, *J. Phys. Chem. A*, 2017, **121**, 717–728.

23 C. Garau, D. Quiñonero, A. Frontera, A. Costa, P. Ballester and P. M. Deyà, *Chem. Phys. Lett.*, 2003, **370**, 7–13.

24 A. Frontera, F. Saczewski, M. Gdaniec, E. Dziemidowicz-Borys, A. Kurland, P. M. Deyà, D. Quiñonero and C. Garau, *Chem. – Eur. J.*, 2005, **11**, 6560–6567.

25 S. E. Wheeler and J. W. G. Bloom, *Chem. Commun.*, 2014, **50**, 11118–11121.

26 A. Bauzá, D. Quiñonero, P. M. Deyà and A. Frontera, *Chem. Phys. Lett.*, 2013, **567**, 60–65.

27 S. E. Wheeler and K. N. Houk, *J. Phys. Chem. A*, 2010, **114**, 8658–8664.

28 J. Zhu, D.-H. Tuo, X.-D. Wang, Y.-F. Ao, Q.-Q. Wang and D.-X. Wang, *Org. Lett.*, 2024, **26**(28), 5984–5988.

29 F. E. Odubo, M. Zeller and S. V. Rosokha, *J. Phys. Chem. A*, 2023, **127**, 5851–5859.

30 T. J. Jentsch, V. Stein, F. Weinreich and A. A. Zdebik, *Physiol. Rev.*, 2002, **82**, 503–568.

31 G. Gil-Ramírez, E. C. Escudero-Adán, J. Benet-Buchholz and P. Ballester, *Angew. Chem.*, 2008, **120**, 4182–4186.

32 S. Kumar, Y. H. Koo, T. Higashino, W. Matsuda, S. Ghosh, Y. Tsutsui, M. Suda, H. Imahori, K. Suzuki, H. Kaji and S. Seki, *Adv. Electron. Mater.*, 2022, **8**, 2101390.

33 H. T. Chifotides, B. L. Schottel and K. R. Dunbar, *Angew. Chem.*, 2010, **122**, 7360–7365.

34 G. Aragay, A. Frontera, V. Lloveras, J. Vidal-Gancedo and P. Ballester, *J. Am. Chem. Soc.*, 2013, **135**, 2620–2627.

35 *TURBOMOLE V7.5 2020 and V7.8 2024 (for SCLH22T), a development of University of Karlsruhe and Forschungszentrum Karlsruhe GmbH, 1989–2007*, TURBOMOLE GmbH, since 2007; available from **https://www.turbomole.org**.

36 R. A. Kendall, T. H. Dunning, Jr. and R. J. Harrison, *J. Chem. Phys.*, 1992, **96**, 6796–6806.

37 F. Weigend, A. Köhn and C. Hättig, *J. Chem. Phys.*, 2002, **116**, 3175–3183.

38 T. H. Dunning, Jr., *J. Chem. Phys.*, 1989, **90**, 1007–1023.

39 H.-J. Werner, P. J. Knowles, G. Knizia, F. R. Manby, M. Schütz, P. Celani, W. Györffy, D. Kats, T. Korona, R. Lindh, A. Mitrushenkov, G. Rauhut, K. R. Shamasundar, T. B. Adler, R. D. Amos, S. J. Bennie, A. Bernhardsson, A. Berning, D. L. Cooper, M. J. O. Deegan, A. J. Dobbyn, F. Eckert, E. Goll, C. Hampel, A. Hesselmann, G. Hetzer, T. Hrenar, G. Jansen, C. Köppl, S. J. R. Lee, Y. Liu, A. W. Lloyd, Q. Ma, R. A. Mata, A. J. May, S. J. McNicholas, W. Meyer, T. F. M. III, M. E. Mura, A. Nicklass, D. P. O'Neill, P. Palmieri, D. Peng, K. Pflüger, R. Pitzer, M. Reiher, T. Shiozaki, H. Stoll, A. J. Stone, R. Tarroni, T. Thorsteinsson, M. Wang and M. Welborn, *MOLPRO, version 2021, a package of ab initio programs*, see **https://www.molpro.net**.

40 F. Weigend and R. Ahlrichs, *Phys. Chem. Chem. Phys.*, 2005, **7**, 3297–3305.

41 F. Weigend, *Phys. Chem. Chem. Phys.*, 2006, **8**, 1057–1065.

42 P. A. M. Dirac and R. H. Fowler, *Proc. R. Soc. London*, 1929, **123**, 714–733.

43 J. C. Slater, *Phys. Rev.*, 1951, **81**, 385–390.

44 J. P. Perdew and Y. Wang, *Phys. Rev. B:Condens. Matter Mater. Phys.*, 1992, **45**, 13244–13249.

45 J. P. Perdew, K. Burke and M. Ernzerhof, *Phys. Rev. Lett.*, 1996, **77**, 3865–3868.

46 J. P. Perdew, M. Ernzerhof and K. Burke, *J. Chem. Phys.*, 1996, **105**, 9982–9985.

47 S. Vosko, L. Wilk and M. Nussair, *Can. J. Phys.*, 1980, **58**, 1200.

48 A. D. Becke, *Phys. Rev. A:At., Mol., Opt. Phys.*, 1988, **38**, 3098–3100.

49 C. Lee, W. Yang and R. G. Parr, *Phys. Rev. B:Condens. Matter Mater. Phys.*, 1988, **37**, 785.

50 A. D. Becke, *J. Chem. Phys.*, 1993, **98**, 5648–5652.

51 T. Yanai, D. P. Tew and N. C. Handy, *Chem. Phys. Lett.*, 2004, **393**, 51–57.

52 Y. Zhao and D. G. Truhlar, *Theor. Chem. Acc.*, 2008, **120**, 215–241.

53 J.-D. Chai and M. Head-Gordon, *Phys. Chem. Chem. Phys.*, 2008, **10**, 6615.

54 A. Wodyński and M. Kaupp, *J. Chem. Theory Comput.*, 2022, **18**, 6111–6123.

55 S. Grimme, J. Antony, S. Ehrlich and H. Krieg, *J. Chem. Phys.*, 2010, **132**, 154104.

56 R. J. Doerksen and A. J. Thakkar, *J. Phys. Chem. A*, 1999, **103**, 10009–10014.

57 V. Gorteau, G. Bollot, J. Mareda and S. Matile, *Org. Biomol. Chem.*, 2007, **5**, 3000.

58 J. Mareda and S. Matile, *Chem. – Eur. J.*, 2009, **15**, 28–37.

59 D.-H. Tuo, Y.-F. Ao, Q.-Q. Wang and D.-X. Wang, *Org. Lett.*, 2019, **21**, 7158–7162.

60 M. R. Battaglia, A. D. Buckingham and J. H. Williams, *Chem. Phys. Lett.*, 1981, **78**, 421–423.

61 G. R. Dennis and G. L. D. Ritchie, *J. Phys. Chem.*, 1991, **95**, 656–660.

62 I. C. Walker, M. H. Palmer and C. C. Ballard, *Chem. Phys.*, 1992, **167**, 61–75.

63 M. A. Spackman, *Chem. Rev.*, 1992, **92**, 1769–1797.

64 L. Miton, E. Antonetti, D. García-López, P. Nava, V. Robert, M. Albalat, N. Vanthuyne, A. Martinez and Y. Cotelle, *Chem. – Eur. J.*, 2024, **30**, e202303294.

65 L. Miton, P.-A. Dupin, E. Antonetti, M. Jean, P. Nava, A. Martinez and Y. Cotelle, *Org. Biomol. Chem.*, 2025, **23**, 4360–4364.

**18004** | *Phys. Chem. Chem. Phys.*, 2025, **27**, 17997–18004

This journal is © the Owner Societies 2025